Gigantic tunneling magnetoresistance in magnetic Weyl semimetal tunnel junctions

D. J. P. de Sousa,[1,*] C. O. Ascencio,[2,†] P. M. Haney,[3] J. P. Wang,[1] and Tony Low[1,‡]

[1]*Department of Electrical and Computer Engineering, University of Minnesota, Minneapolis, Minnesota 55455, USA*

[2]*School of Physics and Astronomy, University of Minnesota, Minneapolis, Minnesota, 55455, USA*

[3]*Physical Measurement Laboratory, National Institute of Standards and Technology, Gaithersburg, Maryland 20899-6202, USA*

(Dated: June 22, 2021)

We investigate the tunneling magnetoresistance in magnetic tunnel junctions (MTJs) comprised of Weyl semimetal contacts. We show that chirality-magnetization locking leads to a gigantic tunneling magnetoresistance ratio, an effect that does not rely on spin filtering by the tunnel barrier. Our results indicate that the conductance in the anti-parallel configuration is more sensitive to magnetization fluctations than in MTJs with normal ferromagnets, and predicts a TMR as large as 10^4 % when realistic magnetization fluctuations are accounted for. In addition, we show that the Fermi arc states give rise to a non-monotonic dependence of conductance on the misalignment angle between the magnetizations of the two contacts.

PACS numbers: 71.10.Pm, 73.22.-f, 73.63.-b

Introduction. Weyl semimetals are novel three-dimensional materials having topologically protected band crossings in the absence of either time reversal (TR) or inversion symmetry (IS) [1–5]. As a result, the low-energy quasi-particles around a given band crossing, or Weyl node, behave as massless Weyl fermions with well-defined chirality determined by its topological charge, i.e., the integrated Berry curvature flux over a surface enclosing the Weyl node [1, 6]. This property is responsible for exotic transport phenomena unique to Weyl semimetals, such as the chiral anomaly [7–10] and the chiral magnetic effect [11, 12]. In magnetic Weyl semimetals [13–16], the strong spin-orbit coupling requires that its magnetization direction is locked to pairs of topological charge dipoles [17]. Associated with each topological charge dipole there is a pair of Weyl sources and sinks with electrons of opposite chirality. Such chirality-magnetization locking gives rise to interesting interplay between electron spins, chirality and magnetization, forming the basis for novel spintronics devices.

In this paper, we study magnetic tunnel junctions (MTJ) comprised of magnetic Weyl semimetal free and reference layers separated by a thin insulating layer. We show that the chirality-magnetization locking of the Weyl semimetal gives rise to a gigantic tunneling magnetoresistance (TMR), where the TMR is defined as $(R_{\rm P}-R_{\rm AP})/R_{\rm P}\times 100$ %, with $R_{\rm P}$ ($R_{\rm AP}$) being the device electrical resistance when the magnetizations of the two contacts are parallel (anti-parallel). The gigantic TMR was found to increase with the momentum space separation of the Weyl nodes, and approach a value of 10^4 % accounting for realistic magnetization fluctuations. In addition, the bulk Weyl and Fermi arc states also results in a non-monotonic dependence of the magnetoresistance on the relative angle between the magnetizations which can, in principle, be detected in experiments.

Chirality-magnetization locking. We employ a standard 4-band lattice model describing a 3D magnetic Weyl semimetal constructed on a cubic lattice of period a, whose effective Hamiltonian is [18, 19]

$$\mathcal{H} = \tau_z \otimes [\mathbf{f}(\mathbf{k})\cdot\boldsymbol{\sigma}] + \tau_x \otimes [g(\mathbf{k})\sigma_0] + \tau_0 \otimes \left(\frac{\beta}{2}\hat{\mathbf{m}}\cdot\boldsymbol{\sigma}\right) \quad (1)$$

where $\mathbf{f}(\mathbf{k}) = \hat{\mathbf{x}}t\sin(k_x a) + \hat{\mathbf{y}}t\sin(k_y a) + \hat{\mathbf{z}}t\sin(k_z a)$ and $g(\mathbf{k}) = t(1-\cos(k_x a)) + t(1-\cos(k_y a)) + t(1-\cos(k_z a))$ are structure factors, $\boldsymbol{\sigma} = \hat{\mathbf{x}}\sigma_x + \hat{\mathbf{y}}\sigma_y + \hat{\mathbf{z}}\sigma_z$ is the vector of Pauli matrices, and $t = 1$ eV is the nearest neighbor

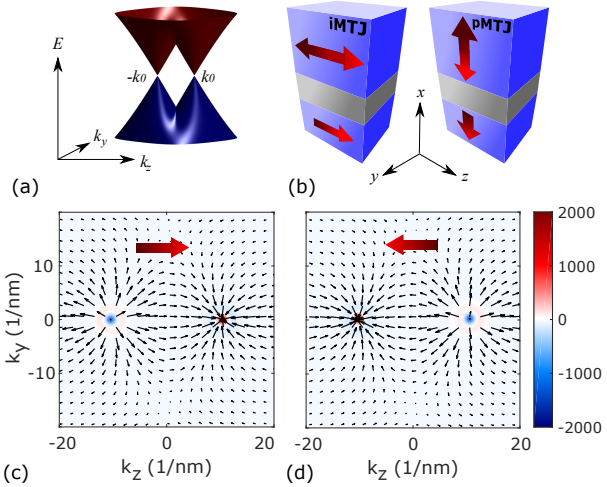

FIG. 1: (a) Typical band structure of a magnetic Weyl semimetal derived from Eq. (1). Here, we assumed an exchange field along the z direction and the following parameters: $\beta = 2$ eV, $t = 1$ eV and $a = 0.1$ nm. (b) in-plane (left) and out-of-plane (right) Magnetic Weyl semimetal tunnel junctions. We will refer to these cases as iMTJ and pMTJ, respectively. Chirality-magnetization locking: The bulk spin texture (vector field) and topological charge (color map) of the conduction band is shown when the magnetization is pointing along (c) +**z** and (d) -**z** direction.

hopping parameter. The Pauli matrices τ (σ) operate in the orbital (spin) space. Finally, $\hat{\mathbf{m}}$ is the unit vector pointing along the magnetization direction with β being the exchange field strength.

Figure 1(a) shows a typical band structure derived from Eq. (1) for $\beta = 2$ eV and $a = 0.1$ nm , for simplicity. We also assume $\hat{\mathbf{m}} = \hat{\mathbf{z}}$ in this case. As shown, we observe a single pair of Weyl nodes located at $\mathbf{k}_0^{\pm} = (0, 0, \pm k_0)$ with $k_0 = (1/a)\arccos\big(1 - \beta^2/(8t^2)\big)$. The MTJ structure is sketched in Fig. 1(b) for two experimentally relevant situations; in-plane (left panel) and perpendicularly magnetized MTJ (right panel). These two configurations will be referred to as iMTJ and pMTJ, respectively. In this system, electrons can tunnel through the barrier with conserved in-plane momentum $\mathbf{k}_{||} = (k_y, k_z)$ due to the translational invariance in the yz-plane and do so with a transmission probability that depends on the angle $\theta_{\rm R}$ between the magnetization of the fixed (bottom) and free (top) layer, $\mathbf{M_L}$ and $\mathbf{M_R}$, respectively. We investigate the dependence of TMR on $\theta_{\rm R}$ in three situations: I) iMTJ with in-plane magnetization rotation; $\mathbf{M_L} = \hat{\mathbf{z}}$ and $\mathbf{M_R}$ rotates in the yz-plane. II) iMTJ with out-of-plane magnetization rotation; $\mathbf{M_L} = \hat{\mathbf{z}}$ and $\mathbf{M_R}$ rotates in the xz-plane and III) pMTJ with out-of-plane magnetization rotation; $\mathbf{M_L} = \hat{\mathbf{x}}$ and $\mathbf{M_R}$ rotates in the xz-plane.

In magnetic Weyl semimetals, the orientation of the topological charge dipole is locked to the direction of the magnetization, giving rise to chirality-magnetization locking [17]. This is due to the strong spin-orbit coupling in these systems and is exemplified in Figs. 1(c) and (d), where we have plotted the spin texture field superposed to the topological charges located at the two Weyl nodes, i.e., $\nabla \cdot \mathbf{\Omega}(\mathbf{k})$ where $\mathbf{\Omega}(\mathbf{k})$ is the Berry curvature, when $\mathbf{M_R} = \pm\mathbf{z}$. Although the Weyl nodes remain at $\mathbf{k}_0^{\pm}$ in both cases, the topological charges and associated spin texture are swapped. Hence, the chirality of electrons with momenta at the vicinity of $\mathbf{k}_0^{\pm}$ reverses sign as $\mathbf{M_R}$ is reversed from $\mathbf{z}$ to $-\mathbf{z}$. Unlike in the parallel magnetization configuration ($\theta_{\rm R} = 0$) where the electrons for each $\mathbf{k}_{||}$ tunnel into states with the same chirality, electrons are unable to conserve $\mathbf{k}_{||}$ while simultaneously maintaining their chirality when the iMTJ is in the antiparallel configuration ($\theta_{\rm R} = \pi$). This chirality-magnetization locking leads to a new chiral TMR and represents a new approach to produce giant TMR unlike what is currently employed in MgO based MTJs which relies on the ability of MgO to filter Bloch states by symmetry and on the half metallic nature of Δ_1 orbital states in magnetic transition metal-based alloys [20]. It is worth emphasizing that a similar effect was predicted to produce large magnetoresistance in magnetic Weyl semimetal domain walls[21].

Theory of chiral tunneling magnetoresistance. We illustrate this mechanism by first considering the tunneling of chiral massless Weyl fermions through an insulating barrier within the context of Bardeen's transfer Hamiltonian approach [22]. For simplicity, we consider an iMTJ with identical Weyl electrodes of Hamiltonians obtained by expanding Eq. (1) to linear order in small wave vector, $\mathbf{q} = (q_x, q_y, q_z)$, around each Weyl node: $\mathcal{H}_e = \hbar v(-i\sigma_x\partial_x + q_y\sigma_y + \chi\cos(k_0 a/2)q_z\sigma_z)$ where x is the transport direction [See Fig. 1(b)]. The chirality index is $\chi = \pm 1$ and v is the Fermi velocity defined as $v = at/\hbar$. Following the Bardeen approach [22–24], we assume that solutions from opposite electrodes are approximately orthogonal everywhere with an exponential tail within the barrier region characterized by an energy independent decay constant κ. We make no assumptions about the shape of the barrier potential, only that it varies slowly compared to the carrier wavelength and that it leads to solutions that are well-localized in the regions of the electrodes. The in-plane translational symmetry allows us to expand our solutions in a basis of Bloch states. The states within the barrier region corresponding to the left (L) and right (R) electrodes read,

$$\Psi^{\xi_{\rm L(R)}}_{\mathbf{q}_{\rm L(R)}}(\mathbf{r}) = C\begin{pmatrix} f^{+}_{\rm L(R)} u^{+}_{\mathbf{q}_{\rm L(R)}}(\mathbf{r}_{||}) \\ i\xi_{\rm L(R)} f^{-}_{\rm L(R)} u^{-}_{\mathbf{q}_{\rm L(R)}}(\mathbf{r}_{||}) \end{pmatrix} e^{i\mathbf{q_L}\cdot\mathbf{r}_{||}} h^{\rm L(R)}(x), \quad (2)$$

where C is a normalization constant [25, 26]. The exponential tail within a barrier of thickness d is captured via $h^{\rm L}(x) = \exp(-\kappa x)$ and $h^{\rm R}(x) = \exp(\kappa(x-d))$ for left and right electrodes, respectively. Additionally, $f^{\pm}_{\rm L(R)} = \sqrt{1 \pm \chi_{\rm L(R)}\lambda_{\rm L(R)}\cos\phi_{\rm L(R)}}$, with chirality and band indeces being $\chi_{\rm L(R)} = \pm 1$ and $\lambda_{\rm L(R)} = \pm 1$ (referring to conduction, +1, and valence, -1, bands), respectively, and $\cos\phi_{\rm L(R)} = \cos(k_0 a/2)q_z^{\rm L(R)}/q_y^{\rm L(R)}$ is given in terms of the in-plane components of the wave vector $\mathbf{q}_{\rm L(R)} = \hat{\mathbf{z}}q_z^{\rm L(R)}\cos(k_0 a/2) + \hat{\mathbf{y}}q_y^{\rm L(R)}$. The periodic part of the in-plane Bloch states $u^{\pm}_{\mathbf{q}_{\rm L(R)}}(\mathbf{r}_{||})$ depends only on the in-plane components of $\mathbf{r}$, i.e., $\mathbf{r}_{||} = (y, z)$. Finally, $\xi_{\rm L(R)} = \lambda_{\rm L(R)}\chi_{\rm L(R)}\,\mathrm{sgn}(q_y^{\rm L(R)})$.

Following Bardeen [22], we derived the matrix element for the tunneling rates [27],

$$M_{LR} = \frac{\hbar^2}{2m}\frac{\alpha_1}{DdS_C}\kappa e^{-\kappa d} \times \left(f_R^- f_L^- + \chi_L\chi_R\lambda_L\lambda_R f_R^+ f_L^+\right)\delta(\mathbf{q}_{\rm L} - \mathbf{q}_{\rm R}), \quad (3)$$

where α_1 is a positive constant related to the overlap between the periodic parts of the in-plane Bloch states from opposite sides of the barrier over a unit cell. In addition, dS_C is the surface area of an in-plane unit cell, and the Dirac delta function is required for in-plane momentum conservation.

We consider the tunneling rates for iMTJs in the parallel $\theta_{\rm R} = 0°$ and anti-parallel configuration $\theta_{\rm R} = 180°$. For simplicity, we assume both Weyl semimetal contacts have the same Fermi level, i.e., $\lambda_{\rm L} = \lambda_{\rm R}$. For the case when the magnetizations are aligned, Weyl nodes with the same chirality on opposite sides of the barrier are

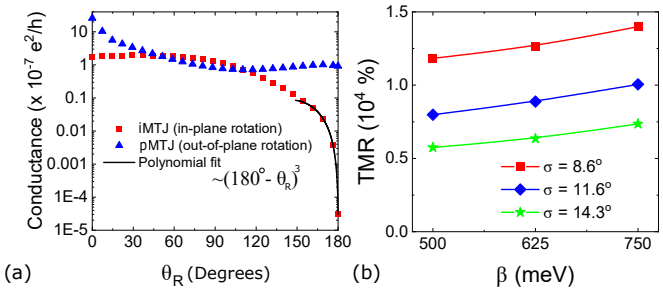

FIG. 2: (a) Angular dependence of the transmission probability (quantum conductance per e^2/h) for pMTJs with out-of-plane rotation (blue triangles) and for iMTJs with in-plane rotation (red squares). The solid black line is a polynomial fit for the iMTJ case at $\theta_{\rm R} \approx 180^\circ$, revealing that conductance of Weyl metal MTJs decays faster than in trivial MTJs. (b) Tunneling magnetoresistance (TMR) ratio as a function of exchange field strength β. Resistances for parallel (anti-parallel) configuration were obtained by convoluting the zero-temperature resistance with a Gaussian kernel of spread σ and center at $\theta_{\rm R} = 0^\circ$ ($\theta_{\rm R} = 180^\circ$), respectively. The spread can be view as due to small thermal fluctuations.

momentum-aligned. The corresponding matrix element becomes $M^{\rm P}_{\rm LR} \sim \frac{\hbar^2}{m}\frac{\alpha_1}{DdS_G}\kappa e^{-\kappa d}\delta(\mathbf{q}_{\rm L} - \mathbf{q}_{\rm R})$. In the anti-parallel configuration, Weyl nodes of *opposite* chirality are momentum-aligned on opposite sides of the barrier. The matrix element for this case with $\chi_{\rm L} = -\chi_{\rm R}$ is $M^{\rm AP}_{\rm LR} = 0$ for all in-plane momenta. These results highlight the immense importance of chirality in the tunneling magnetoresistance of these devices.

Quantum transport results. The analysis above would suggest an infinite TMR in iMTJ based on magnetic Weyl semimetals. In what follows, we will establish that the tunneling magnetoresistance has a much stronger dependence on the relative magnetization angle in the anti-parallel configuration compared to conventional MTJ. Hence, the realistic TMR should be limited by angular fluctuation in magnetization, such as thermal effects [28, 29].

We compute the conductance of the MTJ by means of the non-equilibrium Green's function technique. The Hamiltonian is discretized along the x-direction, i.e., we rewrite Eq. (1) as $\mathcal{H} = H^0_{\rm W} + \hat{W}e^{ik_x x} + \hat{W}^\dagger e^{-ik_x x}$, such that the magnetic Weyl semimetal is described as a series of principal layers (PLs) with translational invariance in the yz-plane, as described by $H^0_{\rm W}$, and connected to its nearest-neighbors PLs via interlayer hopping matrices $\hat{W}$. The Hamiltonian describing the insulating (I) spacer is also expressed in similar fashion, i.e., $\mathcal{H}_{\rm I} = H^0_{\rm I} + \hat{V}e^{ik_x x} + \hat{V}^\dagger e^{-ik_x x}$. The block on-site and hopping matrices are $H^0_{\rm I} = g_{\rm I}(\mathbf{k}_{||})\tau_0 \otimes \sigma_0$, with $g_{\rm I}(\mathbf{k}_{||}) = \epsilon_{\rm I} + t_x + t_y(1 - \cos(k_y a)) + t_z(1 - \cos(k_z a))$, and $\hat{V} = -(t_x/2)\tau_0 \otimes \sigma_0$, respectively. We consider an insulating barrier of three PLs that are coupled to both left (L) and right (R) semi-infinite leads via $H_{\rm L(R)} = -(t_x/2)\tau_0 \otimes \sigma_0$ and assume, $\epsilon_{\rm I} = 2.0$ eV and $t_i = 1$ eV, with $i = x, y, z$ in all regions. The quantum conductance can then be computed using standard non-equilibrium green function formalism fashioned after the Landauer approach to transport [30].

We display in Fig. 2(a) the angular dependence of the conductance in units of e^2/h for both pMTJ and iMTJ with in-plane magnetization rotation. We have assumed $\beta = 500$ meV and a doping level of $\mu = 250$ meV in these calculations. For the iMTJ case (red square symbols), the conductance in the anti-parallel configuration is observed to be orders of magnitude smaller than in the parallel configuration, and is limited by the finite electron damping [30]. Hence, electrons can only transmit if chirality is conserved as elucidated by the Bardeen model.

It is instructive to also consider the pMTJ case, where both magnetizations are in the out-of-plane orientation. In this case, the bulk Fermi surface around different Weyl nodes are projected on the top of one another in the $\mathbf{k}_{||}$-space. As a result, quasi-particles with a given $\mathbf{k}_{||}$ are in coherent superpositions of right- and left- handed states and, therefore, have no well-defined chirality. The full angular dependence of conductance for pMTJs is shown in Figure. 2(a) (blue triangles). Contrary to the iMTJ case, the anti-parallel conductance of pMTJs is only an order of magnitude smaller than its parallel configuration counterpart. The anti-parallel resistances of these two distinct situations, iMTJs and pMTJs, differ by several orders of magnitude, allowing for experimental validation of the proposed physics.

From the analysis above, an ideally infinite TMR ratio should be expected for Weyl iMTJs, as in ideal half-metallic MTJs [32, 33]. However, Fig. 2(a) suggests the conductance exhibits a stronger angular dependence around $\theta_{\rm R} = 180^\circ$. In order to quantify how fast the conductance reaches its minimum value, we have fitted the iMTJ curve of Fig. 2(a) with a polynomial function of the small angular deviations $\theta_{\rm AP}$ around $\theta_{\rm R} = 180^\circ$. We have found that the best fit goes as $\theta^3_{\rm AP}$ [See black solid curve in Fig. 2(a)], which is faster than the $\theta^2_{\rm AP}$ for trivial MTJs [34]. In fact, it can be shown that $M_{\rm LR}(\theta_{\rm AP}) \propto \sin(\theta_{\rm AP}/2)\delta(\mathbf{q}_{\rm L} - \mathbf{q}_{\rm R}(\theta_{\rm AP}))$ in this limit [35], where $\sin(\theta_{\rm AP}/2)$ accounts for spinor wavefunction overlap with an additional angular dependence in the Dirac delta function that accounts for the Fermi surface mismatch of the two contacts due to the magnetization misalignment. The transmission probability is $T = \int d\mathbf{q}_{\rm L} d\mathbf{q}_{\rm R} |M_{\rm LR}(\theta_{\rm AP})|^2 \propto \sin(\theta_{\rm AP}/2)^2 \int d\mathbf{q}_{\rm L} d\mathbf{q}_{\rm R} \delta(\mathbf{q}_{\rm L} - \mathbf{q}_{\rm R}(\theta_{\rm AP}))^2 \propto \sin(\theta_{\rm AP}/2)^2 \sin(\theta_{\rm AP}/2) \approx \theta^3_{\rm AP}$ where the additional $\sin(\theta_{\rm AP}/2)$ describes the angular dependence of the $\mathbf{k}_{||}$-space overlap of the projected bulk Fermi surfaces [35]. Therefore, realistic estimation of the size of the TMR should include thermal effects which gives rise to an angular window around which the magnetization fluctuates [28]. This can be estimated by convoluting the angular dependent conductance with a Gaussian kernel

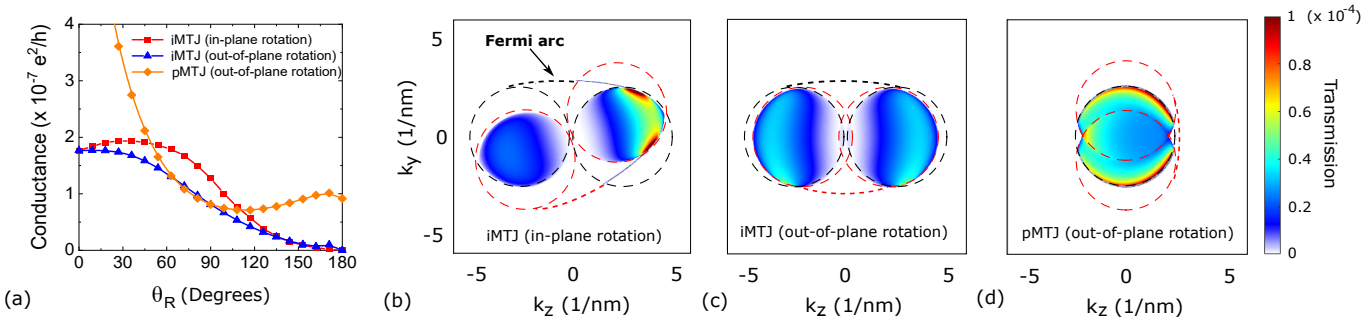

FIG. 3: (a) Angular dependence of the quantum conductance of Weyl semimetal iMTJs with in-plane (red squares) and out-of-plane (blue triangles) magnetization rotations as well as of pMTJs with out-of-plane magnetization rotation (orange rhombus). In these calculations we have selected $\beta = 500$ meV and doping level $\mu = 0.25$ eV measured in relation to the energy location of the Weyl nodes. Panels (b), (c) and (d) show $\mathbf{k}_{||}$-resolved transmission probability at energy $E = 0.0$ eV for $\theta_{\rm R} = 30^\circ$ for each case. The observed transmission hot-spots in panel (b) are due to bulk-to-Fermi arc state tunneling. The dashed contours in figures (b), (c) and (d) highlight the fermi surfaces of left (in black) and right (in red) contacts projected onto the $\mathbf{k}_{||}$-space. Fermi arcs are sketched as dashed lines connecting the bulk Fermi surfaces, as indicated in panel (b).

of spread σ centered around $\theta_{\rm R} = 0^\circ$ and $\theta_{\rm R} = 180^\circ$ for parallel and anti-parallel alignments, respectively. This is justified from the point of view that the magnetization orientation can be described by a Boltzmann distribution $P(\theta_{\rm AP}) = A\exp\left(-K_{\rm eff}\theta_{\rm AP}^2/k_BT\right)$, where A is some normalization constant, $K_{\rm eff}$ is the effective anisotropy coefficient, T is the temperature and k_B is the Boltzmann constant. The Gaussian distribution spread is then $\sigma = \sqrt{k_BT/2K_{\rm eff}}$ [36]. Figure 2(b) shows the TMR obtained from this procedure at different β values for Weyl iMTJs. We observed an additional enhancement with β in all cases. Most importantly, gigantic TMR ratios of $\approx \mathcal{O}(10^4)\%$ are obtained for the range of experimentally relevant σ [29].

We also emphasize that the gigantic TMR ratio of Weyl iMTJs remains robust as long as the chirality around each Weyl node is well-defined. As one increases the doping levels, the Fermi surfaces of the two Weyl nodes merge together, at the so-called Lifshitz transition point in Fig. 1(a), destroying the well-defined handedness of carriers. Under such high doping, we have numerically verified that the anti-parallel resistance becomes finite in this situation and no gigantic TMR ratios are observed. Finally, we also emphasize that the large TMR does not depend on the details of the tunnel barrier [37].

Fermi arc effect. Contrary to MTJs composed of trivial ferromagnetic contacts, where the angular dependence of the conductance obeys $G_0(1+P_{\rm L}P_{\rm R}\cos(\theta))$ with $P_{\rm L(R)}$ being the tunneling spin polarization of the left (right) ferromagnet and G_0 being a multiplicative constant [34], Weyl metal MTJs present a non-trivial anisotropic angular dependence of conductance. This behavior is presented in Fig. 3(a) for pMTJs (orange rhombus) and iMTJs with in-plane (red squared) and out-of-plane (blue triangular) magnetization rotations. Particularly, the conductance of Weyl iMTJs displays a maximum at $\theta_{\rm R} \approx 30^\circ$ when the magnetization is rotated in-plane. To identify the origin of this anomalous behavior, we have analyzed the $\mathbf{k}_{||}$-resolved transmission probability at $\theta_{\rm R} \approx 30^\circ$ for the three cases, as shown in Figs. 3(b), (c) and (d). The red and black dashed circles represent the projection of the bulk Fermi surfaces of right and left contacts, respectively, onto the $\mathbf{k}_{||}$-space. As we rotate the magnetization of the right Weyl contact, its entire bulk Fermi surface rotates along creating a mismatching of momentum states between the two contacts. This accounts for the universal enveloping decreasing conductance with increasing $\theta_{\rm R}$.

Departure from a monotonic decrease of conductance with increasing $\theta_{\rm R}$ can be attributed to the presence of topologically protected Fermi arc states. Due to magnetization misalignment, the surface Fermi arc states can overlap with the bulk states of opposite contact, leading to transmission hot spots as evident in Fig. 3(b). Since these Fermi arc states coexist with the bulk states due to the absence of bulk gap, their wavefunctions generally extend into the bulk [1]. When the magnetization of the right contact in iMTJs is rotated out-of-plane, the bulk-to-Fermi arc mode matching is largely suppressed. Hence, one does not observe any enhancement in the transmission at $\theta_{\rm R} > 0$ [See Fig. 3(c)]. Because tunneling quasi-particles have no well-defined chirality in pMTJs, a small transmission enhancement is allowed to occur for $\theta_{\rm R} > 90^\circ$, as observed in Figs. 3(a) and (d), by virtue of the increasing Fermi surface overlap with minimal Fermi arc mode matching which are counterbalanced by the spinor mismatch only.

Conclusion. We have studied the tunneling magnetoresistance effect in magnetic tunnel junctions comprising of Weyl semimetal contacts. By means of the Bardeen transfer Hamiltonian formalism, we show that the chirality-magnetization locking ensures that the con-

ductance is largely suppressed when the magnetization are perfectly anti-parallel, leading to giant TMR. This result relies on the existence of Weyl nodes with opposite chirality that are separated in the surface Brillouin zone, irrespective of the number of these crossing points. In realistic experimental setup, thermal fluctuations would determines the TMR, and our estimates using realistic magnetization fluctuations indicates a gigantic TMR of order 10^4 %. Numerical quantum transport simulations further reveal the contributions of Fermi arcs surface states, which is reflected in the non-monotonic dependence of conductance on magnetization angle, the signatures of which can offer an avenue to experimentally probe these effects.

Acknowledgments. DS, TL, and JPW were partially supported by the DARPA ERI FRANC program. DS, CA, TL and JPW were partially supported by the SMART, one of two nCORE research centers.

* Electronic address: sousa020@umn.edu
† Electronic address: ascen009@umn.edu
‡ Electronic address: tlow@umn.edu

[1] N. P. Armitage, E. J. Mele and Ashvin Vishwanath, Rev. Mod. Phys. **90**, 015001 (2018).
[2] Shuang Jia, Su-Yang Xu and M. Zahid Hasan, Nat. Mat. **15**, 1140 (2016).
[3] B. Q. Lv, N. Xu, H. M. Weng, J. Z. Ma, P. Richard, X. C. Huang, L. X. Zhao, G. F. Chen, C. E. Matt, F. Bisti, *et. al.* , Nat. Phys. **11**, 724(2015).
[4] Xiangang Wan, Ari M. Turner, Ashvin Vishwanath, and Sergey Y. Savrasov, Phys. Rev. B **83**, 205101 (2011).
[5] A. A. Burkov and L. Balents, Phys. Rev. Lett. **107**, 127205 (2011).
[6] Q. Ma, S.-Y. Xu, C.-K. Chan, C.-L. Zhang, G. Chang, Y. Lin, W. Xie, T. Palacios, H. Lin, S. Jia, *et. al.*,, Nat. Phys. **13**, 842(2017).
[7] A. A. Burkov, Phys. Rev. Lett. **113**, 247203 (2014).
[8] A. A. Burkov, J. Phys.: Condens. Matter **27**, 113201 (2015).
[9] S. A. Parameswaran, T. Grover, D. A. Abanin, D. A. Pesin, A. Vishwanath, Phys. Rev. X **4**, 031035 (2014).
[10] X. Yuan, C. Zhang, Y. Zhang, Z. Yan, T. Lyu, M. Zhang, Z. Li, C. Song, M. Zhao, P. Leng, *et. al.,* Nat. Comm. **11**, 1259 (2020).
[11] M.-C. Chang, M. F. Yang, Phys. Rev. B **91**, 115203 (2015).
[12] U. Dey, S. Nandy and A. Taraphder, Sci Rep **10**, 2699 (2020).
[13] E. Liu, Y. Sun, N. Kumar, L. Muechler, A. Sun, L. Jiao, S.-Y. Yang, D. Liu, A. Liang, Q. Xu, *et. al.,* Nature Physics **14**, 1125(2018).
[14] D. F. Liu, A. J. Liang, E. K. Liu, Q. N. Xu, Y. W. Li, C. Chen, D. Pei, W. J. Shi, S. K. Mo, P. Dudin, Science **365** 1282 (2019).
[15] J. G. Azadani, W. Jiang, J.-P. Wang, Tony Low, Phys. Rev. B **102**, 155144(2020).
[16] W. Jiang, H. Huang, F. Liu, J.-P. Wang, and Tony Low Phys. Rev. B **101**, 121113(R) (2020).
[17] M.P. Ghimire, J. I. Facio, J.-S. You, L. Ye, J. G. Checkelsky, S. Fang, E. Kaxiras, M. Richter, and J. van den Brink Phys. Rev. Research **1**, 032044(R) (2019).
[18] M. Istas, C. Groth, and X. Waintal Phys. Rev. Research **1**, 033188 (2019).
[19] M. M. Vazifeh and M. Franz, Phys. Rev. Lett. **111**, 027201 (2013).
[20] W. H. Butler, Sci. Technol. Adv. Mater. **9**, 014106 (2008).
[21] K. Kobayashi, Y. Ominato, and K. Nomura, J. Phys. Soc. Jpn. **87**, 073707 (2018).
[22] J. Bardeen, Phys. Rev. Lett. **6**, 57 (1961).
[23] M. T. Greenaway, E. E. Vdovin, A. Mishchenko, O. Makarovsky, A. Patanè, J. R. Wallbank, Y. Cao, A. V. Kretinin, M. J. Zhu, S. V. Morozov, *et. al.*, Nat. Phys. **11**, 1057 (2015).
[24] J. R. Wallbank, D. Ghazaryan, A. Misra, Y. Cao, J. S. Tu, B. A. Piot, M. Potemski, S. Pezzini, S. Wiedmann, U. Zeitler, *et. al.*, Science **353**, 575 (2020).
[25] R. M. Feenstra, D. J. Jena, and G. Gu, J. Appl. Phys. **111** 043711 (2012).
[26] L. Britnell, R. V. Gorbachev, A. K. Geim, L. A. Ponomarenko, A. Mishchenko, M. T. Greenaway, T. M. Fromhold, K. S. Novoselov, and L. Eaves, Nat. Commun. **4**, 1794 (2013).
[27] The matrix elements describing the tunneling rates is

$$M_{\rm LR} = \frac{\hbar^2}{2m}\int dS_{x_0}\left\langle \Phi_{\mathbf{q}_{\rm R}}(\mathbf{r}_{||})\middle|\Phi_{\mathbf{q}_{\rm L}}(\mathbf{r}_{||})\right\rangle \times\Big[h_L(x)\frac{dh_R(x)}{dx} - h_R(x)\frac{dh_L(x)}{dx}\Big], \quad (4)$$

with $M_{\rm RL}{}^* = M_{\rm LR}$, m is the effective mass of carriers within the barrier region, $\left|\Phi_{\mathbf{q}_{\rm L(R)}}(\mathbf{r}_{||})\right\rangle$ are the $\mathbf{r}_{||}$ dependent spinor parts of the wave functions, $h_{\rm L(R)}(x)$ are the scalar evanescent parts, and the surface integral is evaluated at $x = x_0$ where x_0 lies inside the barrier.
[28] J. Z. Sun, IBM J. Res. Dev., **50**, 81 (2006).
[29] T. Aoki, Y. Ando,D. Watanabe,M. Oogane and T. Miyazaki, J. Appl. Phys. **103**, 103911 (2008).
[30] The quantum conductance is $G = (e^2/h){\rm Tr}({\rm g}\Gamma_{\rm L}{\rm g}^\dagger\Gamma_{\rm R})$, where broadening functions $\Gamma_{\rm L(R)} = -2{\rm Im}(\Sigma_{\rm L(R)})$ are defined in terms of the self-energies $\Sigma_{\rm L(R)} = H_{\rm L(R)}g_{\rm L(R)}H^\dagger_{\rm L(R)}$, where $g_{\rm L(R)}$ is the retarded surface Green's function of the left (right) Weyl metal lead. Finally, the retarded Green's function for the scattering region, with full Hamiltonian $H_{\rm S}$, is ${\rm g} = (E - H_{\rm S} - \Sigma_{\rm L} - \Sigma_{\rm R} + i\eta)^{-1}$ with $\eta = 10^{-5}$ eV.
[31] In realistic systems, the Weyl nodes separation, $2k_0$, is the real physical parameter to be considered. In general, k_0 is determined by the exchange field strength and the orbital overlap with neighboring sites.
[32] M. Bowen, M. Bibes, A. Barthélémy, J.-P. Contour, A. Anane, Y. Lemaıtre and A. Fert, Appl. Phys. Lett. **82**, 233 (2003).
[33] Y. Sakuraba, M. Hattori, M. Oogane, Y. Ando, H. Kato, A. Sakuma, T. Miyazaki and H. Kubota, Appl. Phys. Lett. **88**, 192508 (2006).
[34] J. C. Slonczewski, Phys. Rev. B **39**, 6995 (1989).
[35] Applying the rotation operator to the spinor eigenstate Eq. (2) and taking the overlap of Eq. (4) considering $\chi_{\rm L} = -\chi_{\rm R}$, we obtain

$$M_{\rm LR}(\theta_{\rm AP}) = i\alpha_1(\kappa\hbar^2/2m)(\cos(k_0a/2)q_z^{\rm L(R)}/\epsilon_k)e^{-\kappa d} \times\delta(\mathbf{q}_{\rm L} - \mathbf{q}_{\rm R}(\theta_{\rm AP}))\sin(\theta_{\rm AP}/2). \quad (5)$$

The angular dependence of the overlap of the Fermi surface projections is proportional to the $\mathbf{k}_{||}$-space overlap area, i.e., $\approx 3k_0k_\mathrm{F}\sin(\theta_\mathrm{AP}/2)$ with k_0 being the Weyl node location and k_F the Fermi wave vector.

[36] From Ref. [17], we have $K_\mathrm{eff} \approx 1.71$ meV per unit cell for the magnetic Weyl semimetal $Co_3Sn_2S_2$. This gives $\sigma \approx 2.08^\circ$ at $T = 172$ K (Curie temperature).

[37] See Supplemental Material at http://link.aps.org/supplemental/xx.xxxx/PhysRevx.xxx for mores details on the influence of the tunnel barrier on the tunneling magnetoresistance ratio size.